Graphene/Na carboxymethyl cellulose composite for Li-ion batteries prepared by enhanced liquid exfoliation

Naboka, Olga; Yim, Chae-Ho; Abu-Lebdeh, Yaser

Publisher's version / Version de l'éditeur:
https://doi.org/10.1016/j.mseb.2016.04.003
Materials Science and Engineering B, 2016-04-24

Materials Science and Engineering B xxx (2016) xxx–xxx

Contents lists available at ScienceDirect

Materials Science and Engineering B

journal homepage: www.elsevier.com/locate/mseb

Graphene/Na carboxymethyl cellulose composite for Li-ion batteries prepared by enhanced liquid exfoliation

Olga Naboka[a,b], Chae-Ho Yim[a,b], Yaser Abu-Lebdeh[a,b,*]

[a] Energy, Mining and Environment Portfolio, National Research Council Canada, 1200 Montreal Road, Ottawa, ON K1A 0R6, Canada
[b] Automotive and Surface Transportation Portfolio, National Research Council Canada, 1200 Montreal Road, Ottawa, ON K1A 0R6, Canada

ARTICLE INFO

Article history:
Received 10 December 2015
Received in revised form 9 April 2016
Accepted 12 April 2016
Available online xxx

ABSTRACT

In the present work, we report a sonication-assisted exfoliation method of graphene preparation enhanced by the use of microwave heating and "green" exfoliant – sodium carboxymethyl cellulose (NaCMC). Introducing microwave heating during sonication of graphite dispersions in aqueous solutions of NaCMC results in the formation of graphene dispersions with concentration as high as 4.29 mg/ml. It is found that drying the dispersions results in the formation of graphene/NaCMC composites with graphene content up to 38.65 wt%. A study of the composite with High Resolution Transmission Electron Microscopy and Raman Spectroscopy reveals the formation of few-layer graphene approximately below five layers. The as-prepared graphene/NaCMC composite shows higher capacities than commercial graphite in Li-ion half cells reaching 397 mAh/$g_{(graphene)}$. Also, when the composite is used with a nanosilicon (33 wt%) in a Li-ion half cell high initial reversible capacities of 1611 mAh/$g_{(Si)}$ with good cyclability and rate capability have been reached.

1. Introduction

Graphene has attracted a lot of attention in recent years due to its outstanding electrical, optical, thermal, and mechanical properties which makes it an ideal choice for many applications ranging from electronics and energy conversion and storage [1–3] to biotechnology and drug delivery [4,5]. In energy storage applications such as batteries and supercapacitors graphene has been considered as an electrode material due to the possibility to optimize the physical and chemical properties of its sheets to obtain high specific surface area, high crystallinity and electronic conductivity, enhanced interaction with other electrode components and electrolyte. In Li-ion batteries, graphene either single or multilayer is able to uptake large amounts of Li ions, even higher than commercial graphite, between the graphene sheets and therefore can be used as an active anode material by itself [3,6–9] or due to its very high electronic conductivity and high aspect ratio (i.e. low percolation threshold ~1 wt%) can be used in a composite as a conductive additive and reinforcing component (both in anode and cathode materials) [6,7,10–12]. Graphene is also very promising for use with Li-ion anode materials undergoing high volume changes during Li uptake such as transition metal oxides, tin and silicon [7,12].

To make the use of graphene commercially viable in Li-ion batteries or for any other application, cost-effective, mass production methods should be developed. There are two approaches to graphene fabrication: top-down one such as the mechanical [13] or chemical graphite exfoliation [14,15], and bottom-up one such as chemical vapor deposition (CVD) of organic precursors [16] or silicon carbide thermal decomposition [17].

Even though the bottom-up approach allows synthesis of highly pure and defect-free graphene, chemical graphite exfoliation is the most promising approach for energy storage applications since it can be relatively easily scaled up at low cost. Graphite can be exfoliated by intercalation [18], oxidation (with subsequent reduction) [15] or sonication in organic solvents or water solutions of surfactants or polymers [14]. Graphene synthesis by chemical functionalization of graphite with intercalating compounds or its oxidation by modified Hummers method is a multistep process consequently resulting in a contaminated and defected product particularly when it comes to graphene oxide [19].

In contrary to chemical functionalization of graphite, graphene produced by sonication in organic solvents (the liquid exfoliation method) is pure and ready-to-use after solvent removal. Irreversible exfoliation of graphite occurs when the surface energy

* Corresponding author at: Energy, Mining and Environment Portfolio, National Research Council Canada, 1200 Montreal Road, Ottawa, ON K1A 0R6, Canada. Tel.: +1 6139494184.
E-mail addresses: olga.naboka@nrc-cnrc.gc.ca (O. Naboka), chae-ho.yim@nrc-cnrc.gc.ca (C.-H. Yim), yaser.abu-lebdeh@nrc-cnrc.gc.ca (Y. Abu-Lebdeh).

http://dx.doi.org/10.1016/j.mseb.2016.04.003
0921-5107/

of the solvent is close to the surface energy of graphite which overcomes Van der Waals forces between graphene sheets [14,20]. Among the best tested solvents are 1-methyl-2-pyrrolidinone (NMP) [20–22] and halogenated aromatic solvents [23,24]. Even though NMP is widely used in the preparation of electrodes for Li-ion batteries which makes it a natural choice, its toxicity and environmental hazard prompted research toward its replacement with environmentally friendly solvents [25,26]. Greener approach for graphite exfoliation was applied by using water solutions of surfactants [27–29]. Surfactants decrease surface tension of water allowing exfoliation and stabilization of graphene dispersions by getting adsorbed at the graphene surface [14]. However, it is almost impossible to purify graphene from surfactant residues. Lotya et al. [27] showed that graphene produced in this way contains up to 40 wt% of residual surfactant (sodium dodecylbenzene sulfonate). Unfortunately such a high amount of inactive component impedes graphene use in battery electrodes.

Acting in a similar way to surfactants, some polymers were shown to be good graphene exfoliants (e.g. polyvinylpyrrolidone [30], poly(vinyl acetate) [31], poly(methyl methacrylate) [31], Gum Arabic [32], ethylcellulose [33], sodium carboxymethylcellulose (NaCMC) [30]). However, similar to surfactants, the final graphene product is expected to be contaminated with polymer. Nevertheless polymer-assisted exfoliation of graphite can still be of interest for Li-ion battery production if graphite exfoliant is chosen to be the same as the polymer binder which is an important component of the electrode to keep all the components adhered together and to the current collector during battery cycling. This will make the whole process of making batteries simpler and more efficient and the polymer to have a dual functionality: exfoliation of graphite to graphene and binding the active materials in the electrode.

Cellulose derivatives are among the most promising polymer candidates for the production of graphene for Li-ion batteries since they are both known to be good binders (especially NaCMC [34]) and to successfully exfoliate graphite [14,30,33]. Graphene/cellulosic composites demonstrate superior mechanical [35] and electrical behavior [36] by themselves which even increases demand for development of cellulose-assisted exfoliation process. In addition to the abovementioned properties cellulose derivatives are renewable and nontoxic materials. However, graphene yield from polymer-assisted exfoliation was reported to be too low to make graphene/polymer composites with reasonable graphene content. For instance, Liang [33] achieved 0.12 mg/ml graphene concentration when using 10 mg/ml (1%, w/v) solution of ethylcellulose. If graphene containing ethylcellulose solution was dried, the final graphene content in polymer composite would be less than 1.2 wt% which is extremely low taking into account that the binder content in electrode formulations usually does not exceed 5–10 wt% and amount of active material should be maximized (~90 wt%). Another drawback of sonication assisted liquid exfoliation of graphite is time consuming: hundreds of hours of sonication are required to get reasonable graphene concentration [21,22,32] which impedes using this method for scalable graphene composite production.

To make the fast direct preparation of graphene/polymer composites with high graphene content possible, the process of polymer-assisted sonication should be improved. From our point of view an increase in the yield and speed of exfoliation can be achieved by using microwave (m/w) heating in addition to ultrasonication since graphene synthesis was reported to be facilitated by m/w heating [37–40] which was applied either for exfoliation of graphite directly [37–39] or for graphite oxide [40]. During m/w irradiation delocalized electrons of graphite can leave the material leading to the ionization of surrounding atmosphere and formation of microplasma spots where the temperature is considerably higher than overall temperature of the system [41] resulting in evaporation of liquid medium. Janowska et al. [37] suggested that water vapors and decomposition products of intercalating compounds significantly increase pressure which we think can give rise to the exfoliation of graphite.

In our work, we used NaCMC as a "green" exfoliating agent for the fast high-yield, water-based graphene preparation that also resulted in a graphene/NaCMC composite. Exfoliation was carried out by combining sonication and m/w heating methods. Since NaCMC is widely used as an electrode binder, graphene/NaCMC composite synthesized by m/w assisted exfoliation can play dual role in electrodes: provide electrochemically active and electronically conductive additive (graphene) and binder (NaCMC). We used synthesized composite as electrochemically active binder to Si nanoparticles since it has been previously shown that graphene made by a liquid exfoliation method is able to improve Li storage capacity of porous single crystalline silicon nanowires [42].

2. Experimental

2.1. Materials

Graphite powder (<45 μm, purity ≥99.99%), sodium carboxymethyl cellulose (NaCMC, average Mw ~ 90,000, 0.7 carboxymethyl groups per anhydroglucose unit, and average Mw ~ 250,000, 0.7 carboxymethyl groups per anhydroglucose unit), ethylene carbonate (anhydrous, 99%), and dimethyl carbonate (anhydrous, 99%+) were purchased from Sigma-Aldrich, monofluoroethylene carbonate – from Solvay, $LiPF_6$ – from Oakwood Chemical. Double deionized water (MiliQ) was used for preparation of water solutions and dispersions. Carbon Super P was purchased from Timcal and stored at 90 °C prior to use. Silicon nanopowder (99%, 100 nm) was purchased from MTI Corporation.

2.2. Preparation of amorphised silicon nanoparticles

Silicon nanopowder was amorphised by ball milling using a SPEX8000 ball mill as reported by reference [43]. A 50 mL tungsten carbide vial (8004, Spex) and two tungsten carbide beads (10.75 g each, Spex) were used along with a powder/ball weight ratio of 1/2; the vials were sealed under an argon atmosphere before milling. The ball milling was performed for 2 h (the time is shorter than in [43] since we used nanosized Si). In order to remove oxide layer from surface of amorphised Si nanoparticles the silicon sample was washed with 50 mL of 1 M HF for 20 min. Sample then was washed with ethanol for five times and dried in vacuum oven at 80 °C overnight. The dried sample was used for further characterization and analysis.

2.3. Graphene preparation

NaCMC solutions with concentrations between 2 and 10 mg/ml were first put into round-neck flasks and to each graphite powder was added at 100 mg/ml. Graphite dispersion in NaCMC was not stable and graphite sedimented directly after preparation. Graphite dispersions were put into an ice-cooled sonicator (VWR, B2500A-MT) and sonicated at 42 (±2.5) kHz and 85 W. After each 1 h of sonication, the flasks were transferred to Microwave Accelerated Reaction System MARS 5 where they were heated under water-cooled reflux during 2 min at 600 W (note: boiling stones were put into the flasks in order to avoid severe dispersion bumping). After heating, the flask was hermetically sealed and allowed to cool down to room temperature (22 (±1) °C) prior to being transferred back to the ice-cooled sonicator. The total sonication time was 10–15 h and samples were m/w heated for 10–15 times (in total 20–30 min).

After exfoliation, the as-prepared graphite/graphene/NaCMC dispersions were left for 3 days in order to sediment large particles

Please cite this article in press as: O. Naboka, et al., Mater. Sci. Eng. B (2016), http://dx.doi.org/10.1016/j.mseb.2016.04.003

then they were transferred to plastic centrifugal tubes and centrifuged at Eppendorf Centrifuge 5702 at 2000–2700 rpm (relative centrifugal force 600–1100 G) during 90 min. Upper 2/3 of supernatant was drawn from test tube and poured into a polypropylene container and left to dry in a convection oven at 80 °C overnight resulting in graphene/NaCMC composite films. The sediment which was mainly made of unexfoliated graphite and some unstabilized graphene and NaCMC residues was neither collected nor further analyzed.

2.4. Examination of graphene with Transmission Electron Microscopy (TEM) and Raman Spectroscopy

High resolution TEM (HRTEM) cannot be performed in the presence of NaCMC because of the degradation of polymer by electron beam.

To prepare samples for TEM and Raman spectroscopy, dried graphene/NaCMC composites were heated under nitrogen flow up to 800 °C (5 °C/min heating rate) and kept at the highest temperature for 1 h. As a result, NaCMC carbonized to amorphous carbon while graphene morphology stayed intact. Carbonized samples were further dispersed in acetone.

Transmission Electron Microscopy (TEM) of dispersions casted on copper grids covered with holey carbon film was performed with FEI Titan 3 80–300 at 300 kV acceleration voltage.

To obtain Raman spectra, samples dispersed in acetone were casted onto Si wafer. The measurements were taken with Renishaw inVia micro-Raman spectrometer at 514 nm. A 50× objective was used. Incident power was 2.5 mW.

2.5. Determination of graphene content in graphene/NaCMC composites by thermogravimetric analysis (TGA)

To determine graphene content in the graphene/NaCMC composite we have made use of the fact that ashing of pure NaCMC in air results in the formation of Na_2CO_3 (Figure S1). Assuming that the weight of ash is proportional to the content of NaCMC in composite – more ash is a result of more NaCMC and less graphene content.

Ashing of samples was performed by TGA (Q 5000-0216, TA instruments) under air flow. Samples were first kept at 110 °C for 1 h in order to remove adsorbed water, then they were equilibrated at 100 °C and heated to 800 °C at 2 °C/min heating rate, then samples were kept for 1 h at this temperature (typical TGA curve for ashing of graphene/NaCMC composite is shown in Figure S2).

2.6. Determination of graphene concentration in dispersion by spectrophotometry

To measure the optical absorbance of graphite/graphene dispersions in NaCMC aliquots were drawn at room temperature (22 (±1) °C) and were diluted 10 times with NaCMC solutions. In order to keep the viscosity of dispersions constant, NaCMC solutions used for dilution were first sonicated and m/w heated for the same time as corresponding graphite dispersions. Diluted dispersions were centrifuged using the Eppendorf Centrifuge 5702 at 2000–2700 rpm (relative centrifugal force 600–1100 G) during 90 min. Centrifuged dispersions were left overnight prior to further measurements. When aliquots were too concentrated for analysis (absorbance coefficient ≥2.0), they were further diluted to achieve 1/4–1/100 concentration of starting dispersion.

Measurement of optical absorbance was performed in Cole Parmer 1200 spectrophotometer at 660 nm in disposable polystyrene cuvettes (1 cm optical pathlength). A corresponding solution of NaCMC was used as reference solution.

Optical absorption coefficient (α) was measured based on the optical absorbance of graphene dispersions that were further dried and their graphene content was determined by TGA. Concentration (C) was measured as [20]:

$$C = \frac{dA}{l\alpha},$$

where d is dilution (4–100), A is optical absorbance, l is optical pathlength [m], and C is concentration of graphene dispersion [g/l].

2.7. Infrared spectroscopy

Fourier transform infrared (FTIR) spectra of graphene/NaCMC composites were recorded with Nicolet 6700 FT-IR in the range 4000–800 cm^{-1} (4 cm^{-1} resolution) in attenuated total reflection (ATR) mode using single bounce diamond crystal; averaging of 32 spectra was applied. The spectrum region of around 1800–2300 cm^{-1} was not used for sample evaluation because of the intrinsic adsorption of diamond in this region. Films of as-prepared composites were investigated without any preparation. Graphs were drawn using logarithmic scale for the wavenumber.

2.8. X-ray diffraction

The X-ray diffraction (XRD) patterns were recorded by Bruker D8 Advance diffractometer. Radiation was generated with an X-ray tube with a Cu anode (Kα radiation, λ = 1.54184 Å) at 40 kV and 40 mA. The 2θ range was 10–60°, and the resolution was 0.05° with 10 s averaging time per step. Phase analysis was performed using ICDD PDF-2 databases (release 2008). Measurement of full width at half maximum (FWHM) was performed after subtracting instrumental broadening using external standard (Si).

2.9. Scanning electron microscopy (SEM)

The morphology of the as-prepared composites was investigated using a JEOL JSM-840A in the secondary electron mode. The samples were sputtered with a gold layer. The acceleration voltage was chosen to be 20 kV.

2.10. Electrochemical testing

Electrochemical performance was studied in half cells versus metallic Li. The electrode was prepared by mixing graphene/NaCMC composite and Carbon Super P in 1:1 weight ratio, or by mixing Si, graphene/NaCMC composite and Carbon Super P in 1:1:1 ratio. When CSP was used as the only active material amount of CSP was 90 wt% and binder amount (NaCMC) was 10 wt%. Double deionized water was used as a dispersion medium. Homogeneous slurry was prepared in planetary centrifugal mixer THINKY ARE-310 operating at 2000 rpm. The slurry was casted onto a copper foil current collector (cleaned with 2.5 wt% HCl solution) using an automated doctor-blade spreader (thickness 150 μm). The cast was dried in air for 2–3 h and then discs (d = 12.5 mm) were punched out and kept at least 24 h in the vacuum oven at 80 °C prior to cell assembling and stored there further in order to prevent oxidation of Si. The final active material load was 0.5–07 mg/cm^2.

2325-type coin cells, purchased from NRC Canada, were assembled under argon in the glove box. A lithium disk (d = 16.5 mm) was used as a negative electrode (counter electrode and reference electrode); 80 μl of 1 M $LiPF_6$ solution in ethylene carbonate: dimethyl carbonate: monofluoroethylene carbonate (45:45:10 volume ratio) was used as an electrolyte. A double layer of the microporous 30 μm thick polypropylene film (Celgard 3501) was used as a separator. Capacity measurements were performed by galvanostatic experiments at multichannel Arbin battery cycler (BT2000). The working electrode was first discharged (lithiated) down to 0.005 V and then

Please cite this article in press as: O. Naboka, et al., Mater. Sci. Eng. B (2016), http://dx.doi.org/10.1016/j.mseb.2016.04.003

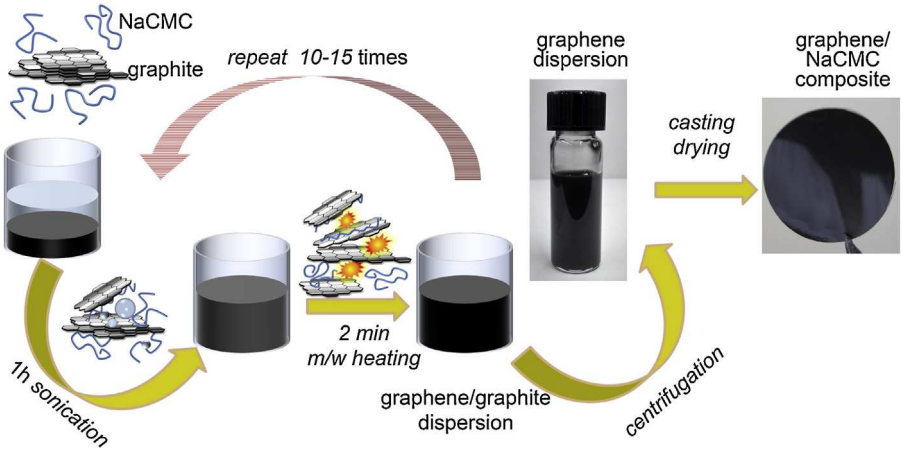

Fig. 1. Schematic of microwave-assisted graphite exfoliation and preparation of graphene/NaCMC composite.

charged (delithiated) to 1.500 V galvanostatically at rates corresponding to currents varying from 17.4 to 348 mA/g per active material (CSP, graphene and/or Si).

3. Results and discussion

3.1. Exfoliation of graphite to graphene

Fig. 1 depicts a schematic of the process used in this work for graphene preparation. Sonication of graphite powder in aqueous solutions of NaCMC leads to the formation of stable black dispersions even at a short period of time of 1 h. The dispersions were found to be stable for a long period of time (for at least 6 months). Drying of dispersions in air resulted in black, glossy free-standing polymer films. The films were brittle and could be easily shattered with little bending, compression or elongation.

TEM image of carbonized polymer films (Fig. 2a) showed that they contain graphene flakes with lateral size in range of ~100–500 nm. The size of flakes correlates well with the values reported elsewhere using a sonication-assisted liquid exfoliation [14,20,23,44]. The thickness of the flakes was assessed with high resolution TEM (HRTEM) of flakes edges. HRTEM reveals folded single layer (Fig. 2b) or few layer (n = 2–5) graphene flakes (Fig. 2b,c).

Raman spectra of graphene and graphite (Fig. 2d) show major peaks around 1360 cm^{-1} (D-band), 1570 cm^{-1} (G-band) and 2700 cm^{-1} (G′-band) [45,46]. The G′-band of the graphene spectrum compared to G-band is much more intense than in graphite which is characteristic for graphene. The shape of G′-band could be assigned to multilayered graphene with less than 5 layers on average (few-layer graphene) [45,46] which agrees with the HRTEM results.

Optical absorbance spectra of graphene dispersions are featureless at the 300–1000 nm range and known to follow Lambert-Beer law at 660 nm [20]. Using TGA of dried graphene/NaCMC composite absorbance coefficients of graphene dispersions in NaCMC90k and NaCMC-250k solutions were calculated to be 2333 $Lg^{-1}\,m^{-1}$ and 3155 $Lg^{-1}\,m^{-1}$ correspondingly. Obtained values are higher than those received by others for water dispersions of graphene either in the presence of surfactants (e.g. sodium dodecylbenzene sulfonate (1390 $Lg^{-1}\,m^{-1}$) [27]) or polymers (e.g. poly(vinyl pyrrollidone) (1293 $Lg^{-1}\,m^{-1}$) [47]). Such difference is most probably caused by influence of stabilizing agents on the optical properties of dispersion (e.g. turbidity). Experimentally obtained absorbance coefficients were used to calculate the concentration of graphene in the dispersion. Fig. 3 shows the concentration of graphene as a function of sonication time and m/w treatment. It is clear that longer sonication time and introduction of m/w heating results in an increase in graphene concentration. For example, sonication of graphite in NaCMC solution (C = 10 mg/ml) for 10 h without m/w heating resulted in a graphene concentration of 1.36 mg/ml. When a m/w heating step for 2 min was introduced after each hour of sonication an increase of graphene concentration to 1.82 mg/ml was obtained corresponding to a 34% increase. Results obtained can be explained by two processes that most probably take place during m/w heating. First one is the formation of local microplasma spots on graphite during irradiation that may result in the evaporation of liquid medium which assist in graphite exfoliation [37,41]. Second one is the exfoliation of graphite by m/w induced oscillation of polar groups of NaCMC which partially intercalate between sheets of graphite during sonication [48]. In addition, the chains of NaCMC stabilize the exfoliated graphene sheets and during further sonication steps move more deeply between graphene sheets which allow more efficient exfoliation during subsequent m/w heat treatment.

The presence of NaCMC is obviously required for the successful graphene preparation since water alone is not expected to exfoliate hydrophobic graphite during ultrasonic treatment [14]. NaCMC stabilizes graphene sterically by getting adsorbed on the graphene sheets thus preventing their re-assembly [31].

In order to maximize graphene/NaCMC ratio in the final composite, the graphene concentration after exfoliation should be as high as possible and at the same time NaCMC concentration should be as low as possible. To improve graphene yield of the liquid exfoliation process we investigated the effect of using NaCMC with higher molecular weight since it is supposed to have better colloid stabilization ability as it was pointed out previously in reference [49]. In this experiment we have also reduced the polymer solution concentration to half from 10 to 5 mg/ml in order to increase the graphene/NaCMC ratio in the final composite which is desirable for battery application. Decreasing the concentration of polymer allowed us to decrease the centrifugation rate from 2700 rpm (1100 G) to 2000 rpm (600 G) due to the lower initial viscosity of the dispersion. As shown in Fig. 4, it is clear that using the higher molecular weight NaCMC-250k results in a significant increase in graphene concentration throughout sonication time. It gave 59% more graphene in solution than when NaCMC-90k was used: 3.7 mg/ml versus 2.2 mg/ml after 9 h of sonication and m/w heating (Fig. 4). 10 h of sonication and m/w heating of graphite in NaCMC-250k resulted in 4.3 mg/ml graphene dispersion. Improvement in the graphene yield may be explained by better stabilizing effect of the longer NaCMC polymer chains – that show better coverage of the graphene sheets leading to stronger repulsive forces [49]. When we compare graphene concentration achieved in solution of NaCMC-90k at 10 mg/ml (Fig. 3) and 5 mg/ml (Fig. 4) it could be seen that a decrease in polymer concentration did not

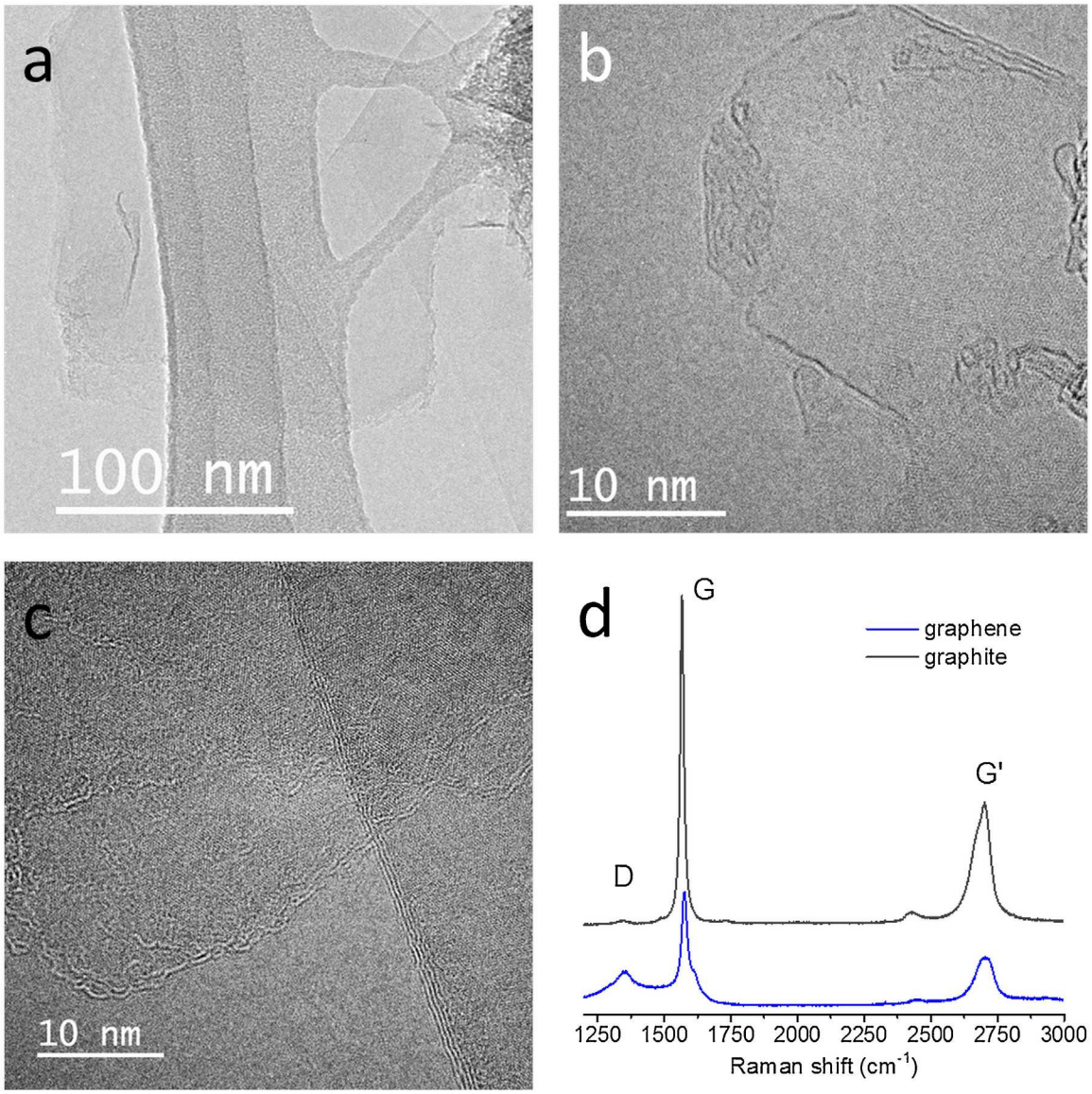

Fig. 2. TEM images of graphene flakes (a–c), (d) Raman spectra of graphene and pristine graphite.

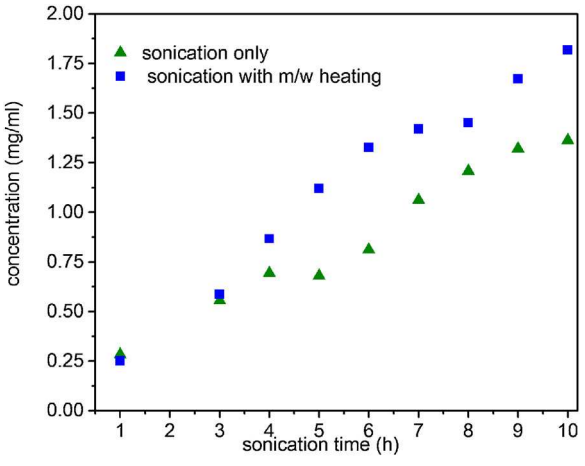

Fig. 3. Concentration of graphene vs sonication time. C(NaCMC) = 10 mg/ml, Mw(NaCMC) = 90,000, centrifugation rate 2700 rpm.

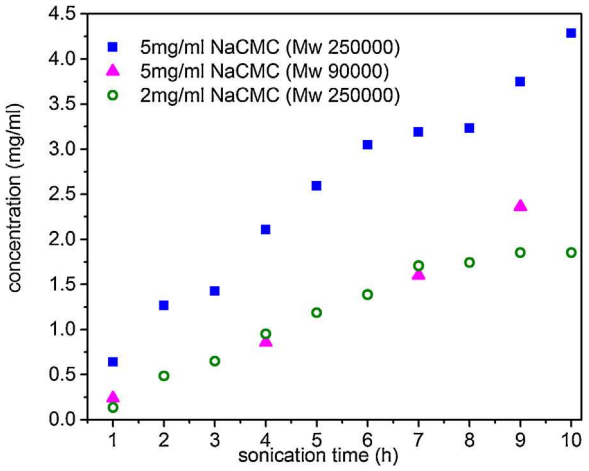

Fig. 4. Concentration of graphene vs sonication time (each hour of sonication was followed by 2 min m/w heating). Note that centrifugation rate was decreased to 2000 rpm due to using lower concentration of NaCMC and therefore lower viscosity of starting solutions.

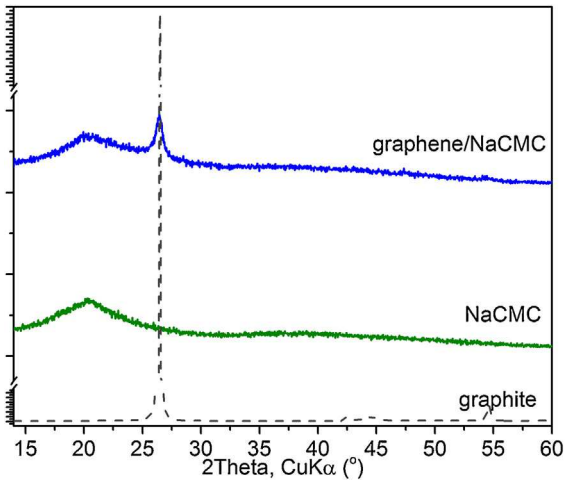

Fig. 5. XRD pattern of graphene/NaCMC composite, NaCMC and graphite.

decrease the final graphene concentration in contrary to what was shown previously with polymers [47] or conventional surfactants [28]. We can even see that graphene concentration after 9 h of sonication in 5 mg/ml solution of NaCMC-90k is 2.36 mg/ml which is higher than the concentration of graphene achieved after 10 h of sonication in 10 mg/ml solution of NaCMC-90k (1.82 mg/ml) (see Table 1 composite 1 and 2). However, the increase in graphene concentration could also be caused by the drop in the centrifugation speed from 2700 (1100 G) rpm to 2000 rpm (600 G). For example, the graphene concentration increased when graphene dispersion in 5 mg/ml solution of NaCMC-250k was centrifuged at 2000 rpm instead of 2700 rpm (Table 1, composite 4 and 5).

In order to optimize graphene/NaCMC ratio the concentration of NaCMC solution was further reduced to 2 mg/ml. However, as it was expected the final graphene concentration was decreased 2.3 times (Fig. 4) which is almost equivalent to the decrease of the NaCMC concentration (2.5 times). The results are consistent with observations made in [47] where concentration of graphene correlated with the concentration of exfoliating polymer. So the highest achieved graphene concentration was 4.3 mg/ml after 10 h of sonication time as shown in Fig. 4. This value is among the highest reported graphene concentrations for a liquid exfoliation process that was obtained in only after 10 h of sonication which is very short time compared to tens and even hundreds of hours reported previously [21,22,32]. Moreover, the yield and concentration of graphene can further be improved by increasing time of sonication and recycling of sediment.

3.2. Graphene/NaCMC composites

Drying of centrifuged dispersions resulted in glossy black films (Fig. 1). XRD patterns of dried dispersions showed the presence of a typical, sharp 002 peak (26.52°, d_{002} = 3.36, FWHM = 0.15) corresponding to a crystalline graphite which is broadened and shifted toward lower 2θ angles (26.44°, d_{002} = 3.37, FWHM = 0.47) compared to starting graphite indicating a decrease in flake thickness (Fig. 5).

SEM images of films revealed the presence of flaky inclusions (Fig. 6a,b, Figure S3) which were absent in pure NaCMC films (Fig. 6c,d). The lateral size of flakes was ~0.1–1.0 μm which agrees with the data obtained by TEM.

Fig. 7 shows the ATR-FTIR spectra of pure NaCMC-250k and exfoliated graphene composite by sonication with and without m/w heating. The NaCMC main bands are assigned to C—H stretch of —CH_2 groups (2915 cm^{-1}) COO^- stretch (1587 and 1411 cm^{-1}),

Table 1
Graphene concentration in solutions and graphene content in graphene/NaCMC composite achieved by sonication and microwave heating of graphite in solutions of NaCMC.

Composite #	MW_{NaCMC}	NaCMC concentration (mg/ml)	Centrifugation rate (rpm)	Absorbance coefficient ($Lg^{-1}\,m^{-1}$)	Total sonication time (h)	Nominal achieved graphene concentration (mg/ml)	Calculated graphene content in graphene/NaCMC composite (wt%)	Final graphene concentration after centrifugation of whole dispersion (mg/ml)	Graphene recovery from whole dispersion (%)	Final graphene content in composite (wt%)
Control (no m/w)	90,000	10	2700	2333	10	1.36	13.41	1.18	86.76	10.55
1		10	2700		10	1.82	15.40	1.41	77.47	12.36
2		5	2000		9	2.36	32.07	2.00	84.75	28.57
3	250,000	2	2000	3155	10	1.85	48.05	1.05	56.63	34.42
4		5	2000		10	4.29	46.18	3.15	73.43	38.65
5		5	2700		15	2.51	33.42	1.74	69.32	25.82

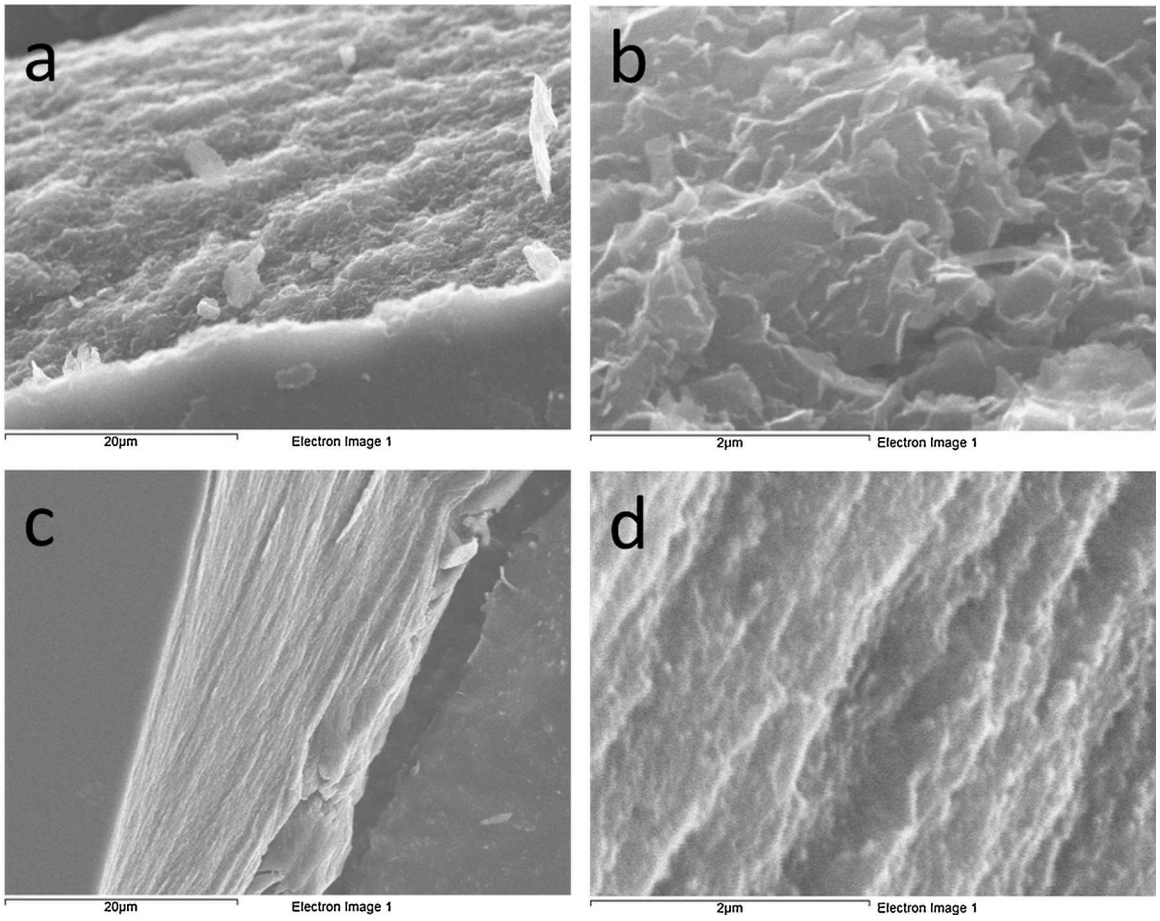

Fig. 6. Graphene/NaCMC composite obtained from sonication of graphite in 5 mg/ml solution of NaCMC (Mw = 250,000) (a,b) and NaCMC film casted from solution of NaCMC (Mw = 250,000) sonicated for 10 h (c, d).

—CCH and —OCH bend (1450 and 1320 cm^{-1}), —CH and —OH coupled bend (1375 cm^{-1}), stretching and bending modes of the bonds within the cellulose backbone (1154, 1105, 1055, 1017 cm^{-1}) [50,51]. A broad band with peak around 3250 cm^{-1} is due to OH-groups and H_2O presence [52]. Graphene/NaCMC composites show less pronounced bands than pure NaCMC which is caused by presence of large amount of graphene. Graphene/NaCMC composites (both prepared by sonication only and by sonication accompanied with m/w heating) show the presence of all bands characteristic to intact NaCMC which suggest that little or no degradation of NaCMC occurred during sonication and m/w heating. FTIR spectroscopy of pure graphene or NaCMC separated from graphene/NaCMC composite is not possible since graphene can not be effectively separated neither by wet chemical method nor by heat treatment because of peculiarities of composite. NaCMC molecules are adsorbed strongly on graphene sheets and cannot be removed from graphene/NaCMC dispersion by precipitation since graphene will be precipitated together with NaCMC; heat treatment of NacMC (carbonization) would lead to formation of amorphous carbon with a lot of functional groups (which would interfere with identification of graphene own functional groups) and change in the structure of graphene.

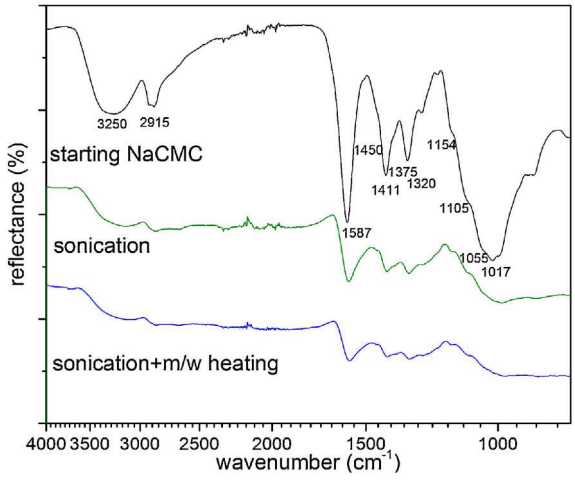

Fig. 7. ATR-FTIR spectra of graphene/NaCMC composites (Mw = 250,000).

The results presented in the previous section deals with the nominal graphene concentration, the concentration measured by spectrophotometry after dilution of the graphene/graphite dispersion with fresh NaCMC solution which was in the range between 1.82 and 4.29 mg/ml. The graphene content in the graphene/NaCMC composites was calculated based on the nominal graphene concentration and the values were in the range between 13.41 and 48.05 wt% that is higher than the actual graphene concentrations measured to be between 10.55 and 38.65 wt% as shown in Table 1. It can be seen that graphene recovery, the ratio of calculated to measured values, lies in the range of 56.63–84.75%. The low recovery could be attributed to weight losses of graphene into the graphite/graphene sediment (pitch) after centrifugation.

Incomplete graphene recovery results in lower graphene content in the composite than it was expected from nominal graphene concentration in dispersion. However, we still obtained

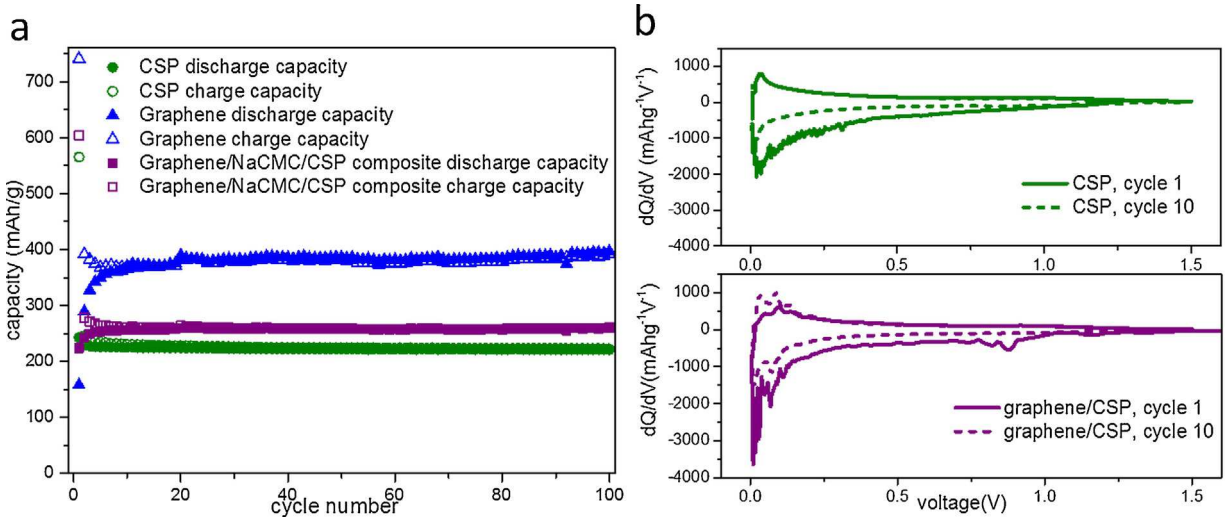

Fig. 8. (a) Cycling performance of graphene/CSP composite, CSP and graphene (CSP contribution to capacity subtracted). Current density 31 mA/g. (b) Differential capacity plots for CSP and graphene/CSP composite.

graphene/NaCMC composite with a high graphene content of 38.65 wt% using NaCMC-250k at 5 mg/ml concentration that will be used as an active material for a Li-ion battery anode. However, even though lower concentration of NaCMC-250k (2 mg/ml) gave similar graphene content (34.42 wt%) and might be another choice, the final amount of its composite is 2.5 times less than in the case of NaCMC-250k at 5 mg/ml concentration and is too low to be used as an anode in a Li-ion battery.

3.3. *Graphene/NaCMC composites as negative electrodes for Li-ion half-cells*

When pure graphene/NaCMC composites casted directly onto a copper current collector and was used as an electrode in a Li-ion half cell (current density 31 mAh/g), it did not show any significant capacity but large polarization (Figure S4). This was most probably caused by the insulating effect of NaCMC due to its coverage and blocking of ion and electron transport from and to the graphene sheets. In order to overcome this insulating action of NaCMC, conductive carbon black (CSP) was used as an additive. Because of high polymer content in our synthesized graphene/NaCMC composite the amount of CSP was maximized. High amount of CSP also helped us to improve mechanical properties of electrode material (NaCMC is a brittle polymer) and prevent it from peeling off from the Cu current collector. CSP is a common carbon additive in battery electrodes and typically used in very low quantities (~5–10 wt%) and therefore its contribution to the bulk capacity is often ignored. Since we used it in large quantities and it is known that it can show electrochemical activity [53,54], it was tested in a half cell as the main active material and using NaCMC as a binder (current density 31 mA/g). It demonstrated a high irreversible capacity (560 mAh/g) and a stable discharge capacity of 221 mAh/g after 100 cycles with 3.5% capacity loss from the second cycle (Fig. 8a, Figure S5) which is similar to results obtained in [53,54].

We then made an electrode with graphene/NaCMC composite (composite 5, see Table 1) and CSP at 1:1 weight ratio. The final content of active materials (graphene and CSP) is 61.25 wt% (13.75 wt% graphene and 47.50 wt% CSP). Prepared electrode was tested in a half cell (current density 31 mA/g). Graphene/CSP composite showed high irreversible capacity (604 mAh/g), followed by stable capacity of 260 mAh/g after 100 cycles (Fig. 8a, Figure S5). We have then subtracted CSP capacity contribution from that of graphene/CSP composite capacity and the results are also shown in Fig. 8a. This demonstrates that in the presence of Carbon Super P graphene shows much more improved discharge capacity of 397 mAh/g after 100 cycles and beyond the first cycle irreversible capacity of 740 mAh/g that is significantly higher than what was previously obtained in our group for commercially available graphene (312 mAh/g) and reduced graphene oxide (217 mAh/g) [55].

Differential capacity (dQ/dV vs. potential) plots of CSP (Fig. 8b, top) show no sharp peaks during the first cycle but gradual increase in current with potential which indicates a gradual formation of solid electrolyte interface. Li-intercalation is completely reversible – it enters and leaves electrode at the same potential on discharge and charge, which is similar to other carbon black studied in [56]. Differential capacity curve for graphene/NaCMC/CSP (Fig. 8b, bottom) shows in addition to features inherent to CSP alone few peaks at low voltages (0.02–0.11 V) both related to the lithium ions intercalation and de-intercalation within the graphitic structure of graphene.

The increase of graphene capacity in the presence of big amount of conductive carbon black supports our assumption that while being efficient exfoliant NaCMC molecules insulate freshly formed graphene sheets from each other and carbon black is required to create conductive paths throughout the graphene/NaCMC composite.

Even though graphene synthesized in our work showed by itself good electrochemical activity, direct use of graphene/NaCMC composite as ready-to-use active electrode material is not practical since it requires high amount of conductive carbon additives.

To test the graphene/NaCMC composite synthesized in our work (sample 4, Table 1) as an electrochemically active binder, it was mixed with Si nanoparticles and CSP in 1:1:1 weight ratio. This ratio was suggested to be optimal by Beattie et al. in [57] in terms of increasing cyclability of Si which can be compromised due to its high volume expansion/contraction as a result of alloying/de-alloying reactions during cycling. The final graphene content was 8.78 wt% and Si content was 33.3 wt%. The electrode was tested in a half cell at different currents ranging between 17.4 and 348.0 mA/g and a voltage range between 0.005 and 1.500 V.

Fig. 9a shows cycling performance of Si in the presence of graphene/NaCMC composite and NaCMC only. Since NaCMC role as a binder may be altered by sonication and m/w heating and might affect the overall capacity of the composite, electrodes containing NaCMC sonicated for 10 h and m/w heated were tested as a control. Charge–discharge curves of composites are presented at Figure S5. To calculate Si specific capacity at various rates, specific capacity

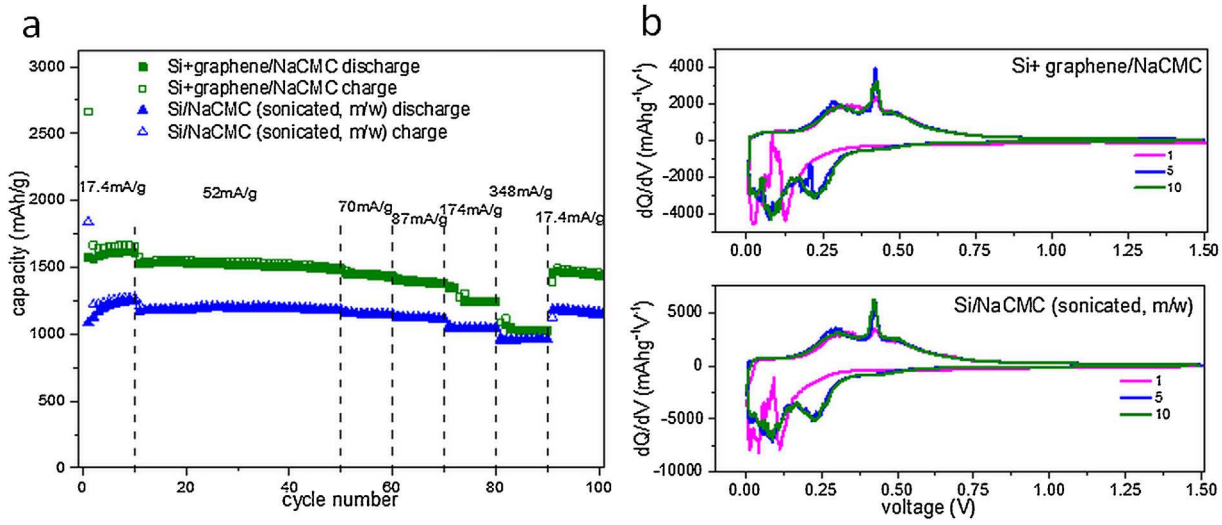

Fig. 9. (a) Cycling performance of Si containing electrodes (graphene and CSP contribution to capacity subtracted). (b) Differential capacity plots for Si containing electrodes.

of CSP and graphene cycled at current density of 31 mA/g was used for subtraction (221 mAh/g and 397 mAh/g correspondingly). Such current density was considered to be small enough to show the specific capacity closest to theoretical. Since contribution of capacity of CSP and graphene to capacity of composite much smaller than capacity of Si, decrease of capacity of CSP and graphene at high currents was neglected.

It can be seen that Si shows the typical high irreversible capacity at the first cycle in the presence of both binders [42,57]. The highest capacity was reached with graphene/NaCMC composite at 1611 mAh/g after 10 cycles, which is almost 30% higher than the capacity of Si electrode in the presence of NaCMC alone (1246 mAh/g) and without graphene. After 100 cycles the Si electrode in the presence of graphene/NaCMC retains 90% of its highest capacity (1439 mAh/g) and still 25% higher than the electrode without graphene.

The differential capacity (dQ/dV) curves of the two Si electrodes (Fig. 9b) are similar and show the two typical lithiation peaks of amorphous silicon in the first cycle around 0.03 V and 0.11 V (shifting to 0.08 and 0.22 V in the second cycle) [58] and two delithiation peaks at 0.42 V and 0.3 V [58]. An increase in the intensity of delithiation peaks with cycling can be observed which points to an improvement in Li ion kinetics [59]. Peaks corresponding to lithiation/delitiation of graphene/CSP composites are obscured by the large capacity of Si.

Si electrode with pure NaCMC binder clearly shows a conditioning effect – increase of capacity with cycling which can be caused by poor compatibility within the electrode as suggested in [43]. Graphene/NaCMC composite conditioning effect is much less pronounced which indicates an improvement of binding properties of NaCMC in the presence of graphene.

The better capacity of the Si electrode in presence of graphene indicates a positive role for graphene in the composite. This can be envisioned by the ability of graphene to mitigate the detrimental effect of volume expansion/shrinking due to its high mechanical strength along with ability to provide a network of conduction pathways [7]. The use of graphene as a conductive additive for battery electrodes has been demonstrated previously and it was shown that due to its high aspect ratio, little amount around 1 wt% is required as a percolation threshold compared to higher amounts for carbon black or even carbon nanotubes [11]. However, in our work the amount of graphene is much higher which means that its role in improving the conductivity could be offset by its ability to uptake lithium ions and contribute to the total capacity. This is corroborated by the fact that the two electrodes showed similar good rate capability as shown also in Fig. 9a. The rate capability of the electrodes was also measured by cycling at higher currents (52, 70, 87, 174, 348 mA/g) and recover at 17.4 mA/g. The capacity retention was excellent and significant decrease was only observed when the rate was ten times the initial current. Even at very high currents (348 mA/g) the reversible capacity for both electrodes was still high and just above 1000 mAh/g, three times more than the capacity of the commercial graphite electrode.

4. Conclusions

In the present work, we prepared graphene/NaCMC composites as anodes for Li-ion battery using a liquid exfoliation method that involves sonication enhanced with microwave heating of graphite dispersions using NaCMC as a water soluble “green” exfoliating agent. It was found that the use of microwave heating along with sonication of graphite dispersions resulted in 34% increase of graphene concentration compared to sonication alone. The exfoliation method was optimized by using NaCMC with high molecular weight (250,000) which resulted in very high yield of graphene in dispersions (4.29 mg/ml) and in graphene/NaCMC composites (38.65 wt%) after only 10 h of sonication. The as-prepared composites were tested as anodes in Li-ion half cells with the help of conductive carbon additive (Carbon Super P) and showed a reversible discharge capacity of 397 mAh/g over 100 cycles. The graphene/NaCMC composite was combined with silicon nanoparticles and gave initial capacities of 1611 mAh/g that decreased to only 1439 mAh/g over 100 cycles.

Acknowledgments

The authors thank Natural Resources Canada for financial support through the Program of Energy Research and Development (Electric Mobility program). The authors wish to thank Mr. David Kingston for SEM micrographs, Dr. Martin Couillard for TEM micrographs and Dr. Christopher Kingston for Raman Spectra.

Appendix A. Supplementary data

Supplementary data associated with this article can be found, in the online version, at http://dx.doi.org/10.1016/j.mseb.2016.04.003.

References

[1] K.S. Novoselov, V.I. Fal'ko, L. Colombo, P.R. Gellert, M.G. Schwab, K. Kim, Nature 490 (2012) 192–200.
[2] N.O. Weiss, H. Zhou, L. Liao, Y. Liu, S. Jiang, Y. Huang, X. Duan, Adv. Mater. 24 (2012) 5782–5825.
[3] D.A.C. Brownson, D.K. Kampouris, C.E. Banks, J. Power Sources 196 (2011) 4873–4885.
[4] I.V. Pavlidis, M. Patila, U.T. Bornscheuer, D. Gournis, H. Stamatis, Trends Biotechnol. 32 (2014) 312–320.
[5] H.Y. Mao, S. Laurent, W. Chen, O. Akhavan, M. Imani, A.A. Ashkarran, M. Mahmoudi, Chem. Rev. 113 (2013) 3407–3424.
[6] S. Han, D. Wu, S. Li, F. Zhang, X. Feng, Small 9 (2013) 1173–1187.
[7] N. Lavoie, F.M. Courtel, P.R.L. Malenfant, Y. Abu-Lebdeh, in: Y. Abu-Lebdeh, I. Davidson (Eds.), Nanotechnology for Lithium-Ion Batteries, Springer, New York, 2013, pp. 117–162 (chapter 6).
[8] Y. Jing, Z. Zhou, C.R. Cabrera, Z. Chen, J. Mater. Chem. A 2 (2014) 12104–12122.
[9] L. Ren, K.N. Hui, K.S. Hui, Y. Liu, X. Qi, J. Zhong, Y. Du, J. Yang, Sci. Reports 5 (2015) 14229.
[10] G. Kucinskis, G. Bajars, J. Kleperis, J. Power Sources 240 (2013) 66–79.
[11] S. Stankovich, D.A. Dikin, G.H.B. Dommett, K.M. Kohlhaas, E.J. Zimney, E.A. Stach, R.D. Piner, S.B.T. Nguyen, R.S. Ruoff, Nature 442 (2006) 282–286.
[12] F. Sun, K. Huang, X. Qi, T. Gao, Y. Liu, X. Zou, X. Wei, J. Zhong, Nanoscale 5 (2013) 8586–8592.
[13] K.S. Novoselov, A.K. Geim, S.V. Morozov, D. Jiang, Y. Zhang, S.V. Dubonos, I.V. Grigorieva, A.A. Firsov, Science 306 (2004) 666–669.
[14] A. Ciesielski, P. Samori, Chem. Soc. Rev. 43 (2014) 381–398.
[15] S. Eigler, A. Hirsch, Angew. Chem. Int. Ed. 53 (2014) 7720–7738.
[16] C.-M. Seah, S.-P. Chai, A.R. Mohamed, Carbon 70 (2014) 1–21.
[17] P.N. First, W.A. de Heer, T. Seyller, C. Berger, J.A. Stroscio, J-S. Moon, MRS Bull. 35 (2010) 296–305.
[18] D.D.L. Chung, J. Mater. Sci. 22 (1987) 4190–4198.
[19] J.P. Rourke, P.A. Pandey, J.J. Moore, M. Bates, I.A. Kinloch, R.J. Young, N.R. Wilson, Angew. Chem. Int. Ed. 50 (2011) 3173–3177.
[20] Y. Hernandez, V. Nicolosi, M. Lotya, F.M. Blighe, Z. Sun, S. De, I.T. McGovern, B. Holland, M. Byrne, Y.K. Gun'ko, J.J. Boland, P. Niraj, G. Duesberg, S. Krishnamurthy, R. Goodhue, J. Hutchison, V. Scardaci, A.C. Ferrari, J. Coleman, Nat. Nanotechnol. 3 (2008) 563–568.
[21] U. Khan, A. O'Neill, M. Lotya, S. De, J. Coleman, Small 6 (2010) 864–871.
[22] U. Khan, A. O'Neill, H. Porwal, P. May, K. Nawaz, J.N. Coleman, Carbon 50 (2012) 470–475.
[23] C.E. Hamilton, J.R. Lomeda, Z. Sun, J.M. Tour, A. Barron, Nano Lett. 9 (2009) 3460–3462.
[24] A.B. Bourlinos, V. Georgakilas, R. Zboril, T.A. Steriotis, A.K. Stubos, Small 5 (2009) 1841–1845.
[25] E. Pohjalainen, S. Räsänen, M. Jokinen, K. Yliniemi, D.A. Worsley, J. Kuusivaara, J. Juurikivi, R. Ekqvist, T. Kallio, M. Karppinen, J. Power Sources 226 (2013) 134–139.
[26] F.M. Courtel, S. Niketic, D. Duguay, Y. Abu-Lebdeh, I.J. Davidson, J. Power Sources 196 (2011) 2128–2134.
[27] M. Lotya, Y.P. Hernandez, J. King, R.J. Smith, V. Nicolosi, L.S. Karlsson, F.M. Blighe, S. De, Z. Wang, I.T. McGovern, G.S. Duesberg, J.N. Coleman, J. Am. Chem. Soc. 131 (2009) 3611–3620.
[28] S.M. Notley, Langmuir 28 (2012) 14110–14113.
[29] S. Vadukumpully, J. Paul, S. Valiyaveettil, Carbon 47 (2009) 3288–3294.
[30] A.B. Bourlinos, V. Georgakilas, R. Zboril, T.A. Steriotis, A.K. Stubos, C. Trapalis, Solid State Commun. 149 (2009) 2172–2176.
[31] P. May, U. Khan, J.M. Hughes, J.N. Coleman, J. Phys. Chem. C 116 (2012) 11393–11400.
[32] V. Chabot, B. Kim, B. Sloper, C. Tzoganakis, A. Yu, Sci. Reports 3 (2013) 1378, http://dx.doi.org/10.1038/srep01378.
[33] Y.T. Liang, M.C. Hersam, J. Am. Chem. Soc. 132 (2010) 17661–17663.
[34] J. Drofenik, M. Gaberscek, R. Dominko, F.W. Poulsen, M. Mogensen, S. Pejovnik, J. Jamnik, Electrochim. Acta 48 (2003) 883–889.
[35] A. Kafy, M. Yadav, K. Kumar, S. Mun, X. Gao, J. Kim, Proc. SPIE 9060 (2014) 906008, http://dx.doi.org/10.1117/12.2044964.
[36] G.W. Jeon, J.E. An, Y.G. Jeong, Composites Part B 43 (2012) 3412–3418.
[37] I. Janowska, K. Chizari, O. Ersen, S. Zafeiratos, D. Soubane, V. Da Costa, V. Speisser, C. Boeglin, M. Houllé, D. Bégin, D. Plee, M.-J. Ledoux, C. Pham-Huu, Nano Res. 3 (2010) 126–137.
[38] V. Sridhar, J.-H. Jeon, I.-K. Oh, Carbon 48 (2010) 2953–2957.
[39] A.M. Shanmugharaj, W.S. Choi, C.W. Lee, S.H. Ryu, J. Power Sources 196 (2011) 10249–10253.
[40] Y. Zhu, S. Murali, M.D. Stoller, A. Velamakanni, R.D. Piner, R.S. Ruoff, Carbon 48 (2010) 2118–2122.
[41] J.A. Menéndez, A. Arenillas, B. Fidalgo, Y. Fernández, L. Zubizarreta, E.G. Calvo, J.M. Bermúdez, Fuel Process. Technol. 91 (2010) 1–8.
[42] X.-L. Wang, W.-Q. Han, ACS Appl. Mater. Interfaces 2 (2010) 3709–3713.
[43] C.-H. Yim, F.M. Courtel, Y. Abu-Lebdeh, J. Mater. Chem. A 1 (2013) 8234–8243.
[44] S. Park, R.S. Ruoff, Nat. Nanotechnol. 4 (2009) 217–224.
[45] A.C. Ferrari, J.C. Meyer, V. Scardaci, C. Casiraghi, M. Lazzeri, F. Mauri, S. Piscanec, D. Jiang, K.S. Novoselov, S. Roth, A.K. Geim, Phys. Rev. Lett. 97 (1–4) (2006) 187401.
[46] L.M. Malard, M.A. Pimenta, G. Dresselhaus, M.S. Dresselahaus, Phys. Rep. 473 (2009) 51–87.
[47] A.S. Wajid, S. Das, F. Irin, H.S.T. Ahmed, J.L. Shelburne, D. Parviz, R.J. Fullerton, A.F. Jankowski, R.C. Hedden, Carbon 50 (2012) 526–534.
[48] P. Lindström, J. Tierney, B. Whathey, J. Westman, Tetrahedron 57 (2001) 9225–9928.
[49] F. He, D. Zhao, Environ. Sci. Technol. 41 (2007) 6216–6221.
[50] J. Wang, P. Soumasundaran, J. Colloid Interface Sci. 291 (2005) 75–83.
[51] L.T. Cuba-Chiem, L. Huynh, J. Ralston, D.A. Beattie, Langmuir 24 (2008) 8036–8044.
[52] A.J. Gordon, R.A. Ford, The Chemist's Companion: a Handbook of Practical Data, Techniques and References, Wiley, New York, 1972.
[53] L. Fransson, T. Eriksson, K. Edström, T. Gustafsson, J.O. Thomas, J. Power Sources 101 (2001) 1–9.
[54] K.-S. Yun, B.-R. Kim, E. Noh, H.-J. Jung, H.-J. Oh, W.-S. Kang, S.-C. Jung, S.-T. Myung, S.-J. Kim, Jpn. J. Appl. Phys. 52 (2013) 11NM01.
[55] N. Lavoie, P.R.L. Malenfant, F.M. Courtel, Y. Abu-Lebdeh, I.J. Davidson, J. Power Sources 213 (2012) 249–254.
[56] A.K. Sleigh, U. von Sacken, Solid State Ionics 57 (1992) 99–102.
[57] S.D. Beattie, D. Larcher, M. Morcrette, B. Simon, J. Electrochem. Soc. 155 (2008) A158–A163.
[58] M.N. Obrovac, L.J. Krause, J. Electrochem. Soc. 154 (2007) A103–A108.
[59] A. Magasinski, P. Dixon, B. Hertzberg, A. Kvit, J. Ayala, G. Yushin, Nat. Mater. 9 (2010) 353–358.

Please cite this article in press as: O. Naboka, et al., Mater. Sci. Eng. B (2016), http://dx.doi.org/10.1016/j.mseb.2016.04.003